

All-Solution-Processed Metal-Oxide-Free Flexible Organic Solar Cells with Over 10% Efficiency

Wei Song, Xi Fan,* Bingang Xu, Feng Yan, Huiqin Cui, Qiang Wei, Ruixiang Peng, Ling Hong, Jiaming Huang, and Ziyi Ge*

All-solution-processing at low temperatures is important and desirable for making printed photovoltaic devices and also offers the possibility of a safe and cost-effective fabrication environment for the devices. Herein, an all-solution-processed flexible organic solar cell (OSC) using poly(3,4-ethylenedioxythiophene):poly(styrenesulfonate) electrodes is reported. The all-solution-processed flexible devices yield the highest power conversion efficiency of 10.12% with high fill factor of over 70%, which is the highest value for metal-oxide-free flexible OSCs reported so far. The enhanced performance is attributed to the newly developed gentle acid treatment at room temperature that enables a high-performance PEDOT:PSS/plastic underlying substrate with a matched work function (≈ 4.91 eV), and the interface engineering that endows the devices with better interface contacts and improved hole mobility. Furthermore, the flexible devices exhibit an excellent mechanical flexibility, as indicated by a high retention ($\approx 94\%$) of the initial efficiency after 1000 bending cycles. This work provides a simple route to fabricate high-performance all-solution-processed flexible OSCs, which is important for the development of printing, blading, and roll-to-roll technologies.

Organic solar cells (OSCs) have attracted enormous attention due to the great potentials of high flexibility, light weight, low cost, and printing and roll-to-roll manufacturing.^[1–8] By now, most of the research results of OSCs with high performance have been reported based on the rigid glass substrates. Concerning the practical commercial application, flexible organic solar cells deserve more investigation for their market penetration as printable, portable, and wearable electronics. A common flexible OSC is composed of active layers sandwiched between a modified flexible transparent electrode (FTE) as an anode and

a low work function metal cathode. The ultimate objective of the field is to develop highly efficient, flexible, and low cost photovoltaic modules via printing, roll-to-roll manufacturing, etc.^[9] Printed flexible devices require that materials can be processed into a liquid, solution, or paste, and the devices will not become widespread until they are cheap and safe enough to fabricate.^[4] Therefore, efforts should be made to improve the device performances and also scale up the solution manufacturing of flexible OSCs for practical implementation. An all-solution-processing at a low temperature (low-*T*) is very suitable for the printing, roll-to-roll manufacturing, and blading, and will also make the flexible productions cost-effective.

In the OSCs, the most popular electrodes are metal doped metal oxides (MMOs), such as indium doped tin oxide (ITO). However, ITO suffers from mechanical brittleness and conductivity issues on plastic substrates.^[10–12] Moreover, metal oxide films are commonly processed via vacuum sputtering at high temperatures which renders the MMO films expensive^[13–16] and is incompatible with printing and roll-to-roll manufacturing. Several emerging materials have been reported as candidates of the sputtered MMO films, including conducting polymers,^[17–22] carbon nanotubes,^[23–25] graphene,^[6,26–28] metallic nanowires,^[29–31] metallic grids,^[32,33] and hybrid films.^[34–36] Among them, poly(3,4-ethylenedioxythiophene):poly(styrenesulfonate) (PEDOT:PSS) films afford the relatively low cost and the films exhibit high optical and electrical characteristics, excellent thermal stability, good flexibility, etc.^[20–22,37,38] For instance, Xia et al. and Kim et al. reported an innovative H₂SO₄ treatment at 160 °C^[20] and at room temperature (room-*T*),^[22] respectively, which improved significantly the conductivity (σ) of PEDOT:PSS to three orders of magnitude (from 1 to over 3000 S cm⁻¹). Using the PEDOT:PSS, rigid devices with P3HT:PCBM and PTB7:PC₇₁BM exhibited a power conversion efficiency (PCE) of 3.56% and 6.7%, respectively. Then, Kim et al. reported a unique H₂SO₄ assisted transfer-printing technique that realized a PEDOT:PSS film with super-high conductivity of 4000 S cm⁻¹.^[38] Flexible devices (area: 4.64 mm²) with PTB7-Th:PC₇₁BM yielded a higher PCE of 7.7% with superior durability as compared with ITO-based devices. Kang et al. reported flexible OSC (area: 4.64 mm²) with polyethyleneimine

W. Song, Prof. X. Fan, H. Q. Cui, Q. Wei, R. X. Peng, L. Hong, J. M. Huang, Prof. Z. Y. Ge
Ningbo Institute of Materials Technology and Engineering
Chinese Academy of Sciences
Ningbo 315201, China
E-mail: fanxi@nimte.ac.cn; geziyi@nimte.ac.cn

Prof. B. G. Xu, Prof. F. Yan
Institute of Textiles and Clothing
Department of Applied Physics
The Hong Kong Polytechnic University
Hung Hom, Kowloon, Hong Kong 999077, China

 The ORCID identification number(s) for the author(s) of this article can be found under <https://doi.org/10.1002/adma.201800075>.

DOI: 10.1002/adma.201800075

(PEI)/Ag (9 nm)/PEDOT:PSS hybrid FTEs.^[39] Flexible devices with PTB7-Th:PC₇₁BM exhibited the highest PCE up to 9.9%, which brought flexible OSCs close to commercialization. We recently reported a flexible OSC (area: 6.0 mm²) using a transferred PEDOT:PSS FTE.^[40] Flexible device with PBDTT-S-TT:PC₇₁BM showed a PCE of 6.42%. Therefore, PEDOT:PSS is critical to the performances of the OSCs.

Although strong acid treatments are capable of dramatically improving the conductivity of PEDOT:PSS films, most strong acid treatments are incompatible with plastic underlying substrates because of a large-domain damage of the plastic substrates in the harsh strong acid processing especially at a high temperature (high-*T*). To prepare a highly conductive PEDOT:PSS FTE and simultaneously to avoid destroying the plastic underlying substrates, a route is to use the transfer-printing methods.^[38,40] However, a feasible transfer-printing required rather complex processing and the recipes are suffered from low yields of large-area productions,^[21,40] due to a great challenge of precisely controlling interface adhesion. The other route is to prepare hybrid structures of metal/PEDOT:PSS doped with secondary solvents.^[34,39] However, the PEDOT:PSS films commonly showed modest conductivity of 500–1000 S cm⁻¹. In addition, the aqueous PEDOT:PSS dispersion is acidic at pH 1 and corrosive to the underlying metals, possibly deteriorating the device performances. Whereas low-*T* gentle acid treatments provide a simple pathway for making a desirable PEDOT:PSS FTE and simultaneously avoiding the damages of plastic substrates thanks to a weak destructive property of gentle acids at low-*T*. Moreover, unlike the powerful oxidizing H₂SO₄ and HNO₃ solutions that destroyed severely the polyethylene terephthalate (PET) (see Figure S1, Supporting Information), the gentle acids without powerful oxidizing property are perhaps suitable to treat PEDOT:PSS at low-*T*, improving the film conductivity, and protecting the plastic underlying substrates. Those motivate us to explore simple strategies for making high-performance all-solution-processed flexible OSCs.

Herein, we demonstrate an efficient all-solution-processed metal-oxide-free flexible OSC with PEDOT:PSS/PET substrates treated by methanesulfonic acid (CH₄SO₃) at room-*T*. The gentle acid treatments at room-*T* (≈20 °C) induced a smooth and uniform PEDOT:PSS film with high optical and electrical characteristics. Unlike harsh treatments of

H₂SO₄ and HNO₃, the room-*T* gentle acid treatment avoids destroying the plastic underlying substrates, and thus it is compatible with the underlying plastic substrates. More encouragingly, except the Al cathodes that must be deposited thermally, all the components of the flexible OSC devices are solution-processed at lower temperatures of no more than 100 °C, which is a convenient approach and compatible with printing and roll-to-roll manufacturing. The all-solution-processed flexible devices exhibited the best PCE of 10.12% with *V*_{OC} of 0.93 V, *J*_{SC} of 15.49 mA cm⁻², and fill factor (FF) of 70.27%. To the best of our knowledge, it is the highest PCE for solution-processed metal-oxide-free flexible OSCs reported so far. And the flexible devices retained ≈94% of the initial PCE after 1000 cycle continuous bending tests (bending radius, *r* = 5.6 mm). Furthermore, when the all-solution-processed devices were fabricated on glass substrates, showing a higher efficiency up to 10.60%. The all-solution-processing at low temperatures is suitable for printing, roll-to-roll manufacturing, and blading/shearing for making high-efficiency OSC devices.

We first prepared a series of PEDOT:PSS films on the plastic substrates of PET with acid treatments at room-*T* and compared their conductivities in Table S1 of the Supporting Information). It is found that the highest conductivity of the films is achieved by 99 wt% CH₄SO₃ and 68 wt% HNO₃ treatments at room-*T* for 10 min. When the duration of CH₄SO₃/HNO₃ processing time is over 10 min, film conductivity did not increase and became consistent. Figure 1a plots all the values of conductivity and square resistance (*R*_{sq}) of the PEDOT:PSS/PET substrates. Moreover, the 98 wt% H₂SO₄ treatments dissolved the PET underlying substrates in a short time of 5 min (see Figure S1, Supporting Information), thereby the harsh H₂SO₄ treatments are incompatible with the plastic substrates. A 68 wt% HNO₃ made the PET substrates fragile and caused a decreased optical transparency in the acid processing of over 10 min, which was probably resulted from the strong oxidant and powerful corrosive properties of the HNO₃. CH₄SO₃ is a gentle acid without powerful oxidizing property though the CH₄SO₃ solutions would destroy severely the PET at high-*T* (over 120 °C). At room-*T*, however, the CH₄SO₃ solution is quite mild and it avoids the large-domain damages of the PET. Therefore, the CH₄SO₃ treatment at room-*T* is used to treat the PEDOT:PSS/PET substrates.

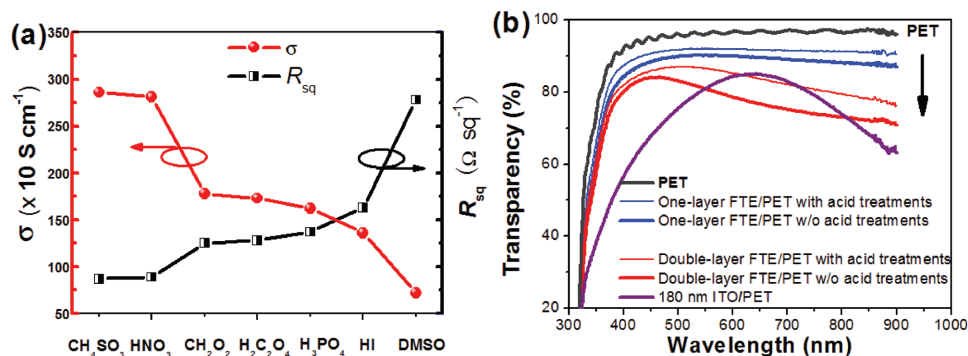


Figure 1. a) Comparison of square resistance and electrical conductivity of the PEDOT:PSS with diverse acid treatments at room-*T* and DMSO doping. b) Transparency spectra of PET substrates (≈200 μm), PEDOT:PSS/PET and ITO/PET substrates.

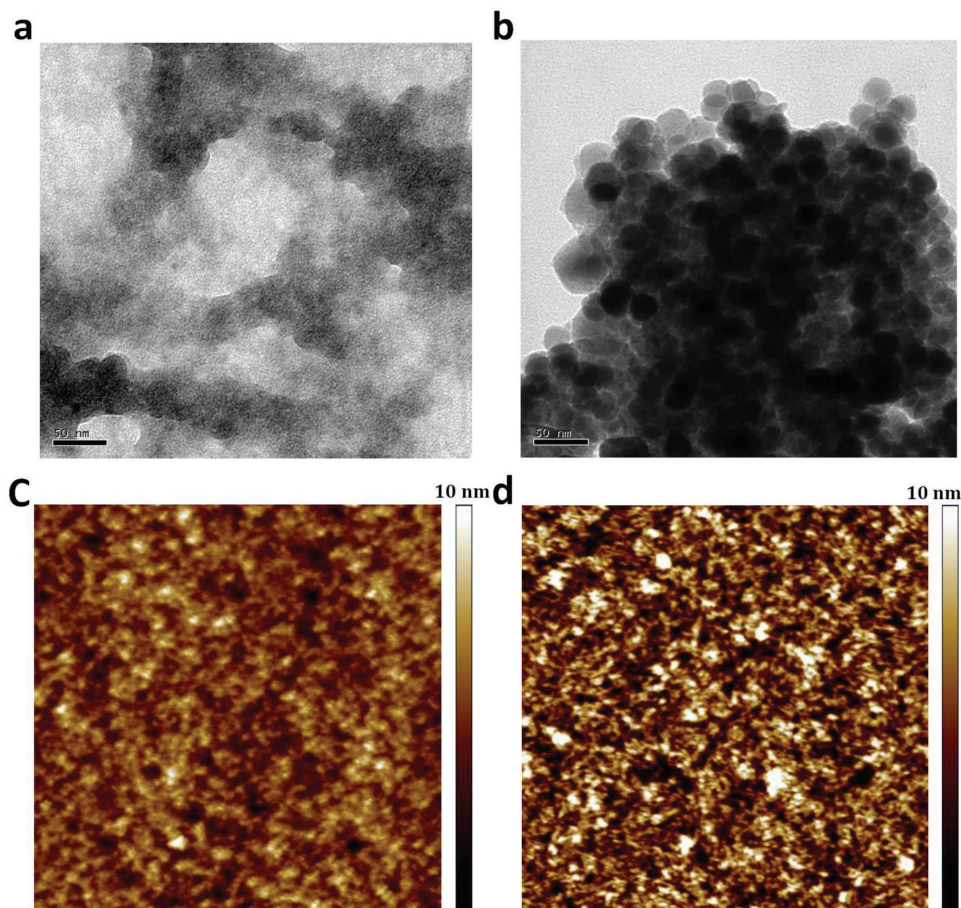


Figure 2. TEM images of the PEDOT:PSS films: a) pristine films, and b) the films with the room-*T* gentle acid treatments. AFM images of the PEDOT:PSS films on PET plastic substrates: c) pristine films, and d) the films with the room-*T* gentle acid treatments. Scale bar: $2 \times 2 \mu\text{m}^2$.

Figure 1b shows transparency spectra of the pristine films and the films with the CH_4SO_3 treatments at room-*T*. Obviously, a higher transparency in the region of $\lambda \geq 400 \text{ nm}$ is observed in the films with the acid treatments. The highly transparent films are resulted from a removal of hydrophilic PSS from PEDOT:PSS matrix and a better stack of PEDOTs induced by the acid treatments. It had been reported that after the treatments of HNO_3 and H_2SO_4 ,^[16,22] PEDOT:PSS films on glass substrates became more transparent in the region of $\lambda \geq 520 \text{ nm}$. Thus, the transparent films can save the incident lights for an active absorption.

The room-*T* gentle acid treatment plays a significant role on the morphology evolution of the films. **Figure 2** shows the transmission electron microscopy (TEM) images of the pristine films and the films with the 99 wt% CH_4SO_3 treatments. In Figure 2a, no obvious aggregates of PEDOT:PSS were found in the pristine films. After the gentle acid treatments at room-*T*, a number of small aggregates appeared and were well connected (see Figure 2b), suggesting a better phase separated morphology. The aggregates were induced by the gentle acid treatments that enabled the as-cast PEDOT coiled structures to transform linear/extended-coil structures, leading to more interchain interactions among the PEDOTs for an enhanced conductivity. It is notable that the PEDOT

aggregates were uniform and continuous and showed a smaller particle size of 20–40 nm as compared with that ($\approx 100 \text{ nm}$) of large-domain PEDOT aggregates with high-*T* CH_4SO_3 treatments reported before,^[19] which facilitated the penetration of H^+ into the PEDOT:PSS matrix and to combine the insulating PSS^- ($\text{PSS}^- + \text{H}^+ \rightarrow \text{PSSH}$) for making a highly conductive and smooth PEDOT:PSS FTE.

Figure 2c,d shows the atomic force microscopy (AFM) images of the pristine films and the films with the room-*T* gentle acid treatments. The pristine film showed a high smoothness with a root-mean-square (RMS) of 1.67 nm. However, the film was suffered from a poor phase separated morphology. After the gentle acid treatments, the film exhibited a well-distributed and uniform phase separated morphology with RMS of 2.14 nm, which made conducting PEDOT chains interconnecting well for charge hopping, eventually contributing to a tremendous enhancement in conductivity. It should be notable that the room-*T* acid treatments differ from the high-*T* acid treatments at 120–160 °C reported before.^[19,37,41] High-*T* CH_4SO_3 solutions would destroy the PET plastic substrates and cause a rough PEDOT:PSS film (RMS: 4.0–6.7 nm).^[19,37] Moreover, the high-*T* CH_4SO_3 treatments would result in a poor flexibility of OSC devices just with 100 cycle bending,^[37] and a much lower PCE of flexible solar cells as compared with ITO-based devices.^[41]

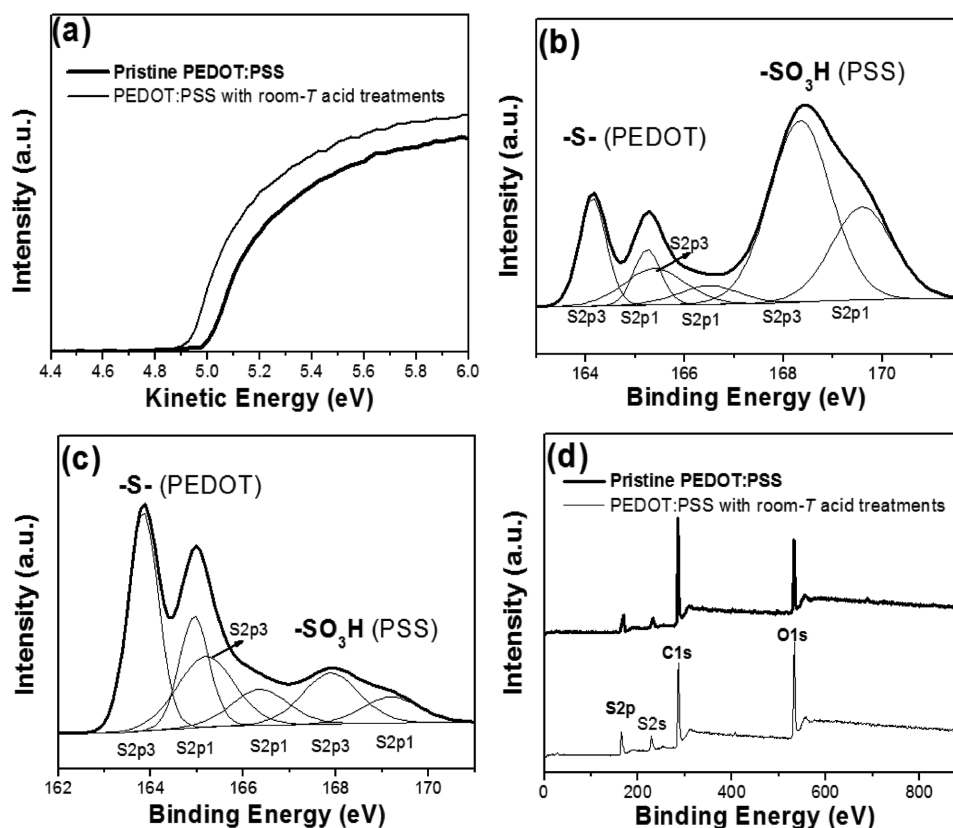


Figure 3. a) UPS spectra of the pristine films and the films of PEDOT:PSS with the room-*T* gentle acid treatments. b,c) Fitted S 2p XPS spectra of the pristine films (b) and the acid-treated films (c). d) XPS spectra of both the films.

Apart from the enhanced optical and electrical characteristics and better morphology of the PEDOT:PSS film induced by the room-*T* gentle acid treatments, the work function (WF) and surface element components are investigated. Here, ultraviolet photoelectron spectroscopy (UPS) is used to probe the WF values of the as-cast PEDOT:PSS film and the PEDOT:PSS film with room-*T* gentle acid treatments, as shown in **Figure 3a**. Obviously, the WF (−4.91 eV) of PEDOT:PSS films with the room-*T* CH₄SO₃ treatments matches well with the WF (−5.05 eV) of PEDOT:PSS (4083) buffer layers and the valence-band edge (−5.21 eV) of poly[(2,6-(4,8-bis(5-(2-ethylhexyl)thiophen-2-yl)benzo[1,2-*b*:4,5-*b'*])dithiophene)-*co*-(1,3-di(5-thiophene-2-yl)-5,7-bis(2-ethylhexyl)benzo[1,2-*c*:4,5-*c'*])dithiophene-4,8-dione)] (namely, PBDB-T) for hole transport and extraction by the electrodes. Moreover, as compared with the WF (−4.80 eV) of PEDOT:PSS with high-*T* CH₄SO₃ treatments,^[41] the appropriate WF (−4.91 eV) of PEDOT:PSS with the room-*T* CH₄SO₃ treatments can induce a smaller potential barrier for making better solar cells.

X-ray photoelectron spectroscopy (XPS) is an effective way to probe atom contents and element states of PEDOT:PSS. The XPS bands with the binding energies (BEs) of 166–172 eV originated from the sulfonate moieties of PSS; and the XPS bands with the BEs of 162–166 eV originated from the thiophene rings of PEDOT. **Figure 3b,c** shows the S 2p of XPS spectra of the pristine films and the films with the room-*T* CH₄SO₃ treatments, respectively. It presents that the ratio of the S of −SO₃H

originated from PSS to total S atoms is 68.6 at% for the pristine films. After acid treatments, the peak of the S of −SO₃H became weaker and the peak of −S− originated from PEDOT became stronger, demonstrating the removal of PSS from PEDOT:PSS matrix. The ratio of the S of −SO₃H is decreased to 45.7 at% for the films with the gentle acid treatments. Moreover, the concentration of S is increased from 8.55 to 9.42 at% calculated from the full XPS spectra in **Figure 3d**, because of a rearrangement of PEDOT:PSS films with the removal of PSS,^[20,22,37,38] contributing to the enhancement of film conductivity. Owing to the high optical and electrical characteristics, the smooth and uniform morphology, and the matched WF, the PEDOT:PSS/PET substrates are suitable to make high-efficiency flexible solar cells as an FTE.

On the basis of the PEDOT:PSS/PET substrates, we fabricated the all-solution-processed flexible OSCs with a structure of PET/PEDOT:PSS FTE/PEDOT:PSS buffer layer/PBDB-T:methyl-substituted 3,9-bis(2-methylene-(3-(1,1-dicyanomethylene)-indanone)-5,5,11,11-tetrakis(4-hexylphenyl)-dithieno[2,3-*d*:2',3'-*d'*]-s-indaceno [1,2-*b*:5,6-*b'*]-dithiophene (namely IT-M)/Perylene diimide amino N-oxide (PDINO)/Al (see **Figure 4a**), where, the polymer PBDB-T is used as an electron donor and the IT-M is used as an electron acceptor. The molecular structures of PEDOT:PSS, PBDB-T, IT-M, and PDINO are shown in **Figure S2** of the Supporting Information. **Figure 4b** shows the energy levels of the components of the flexible devices, ITO films, and PEDOT:PSS films

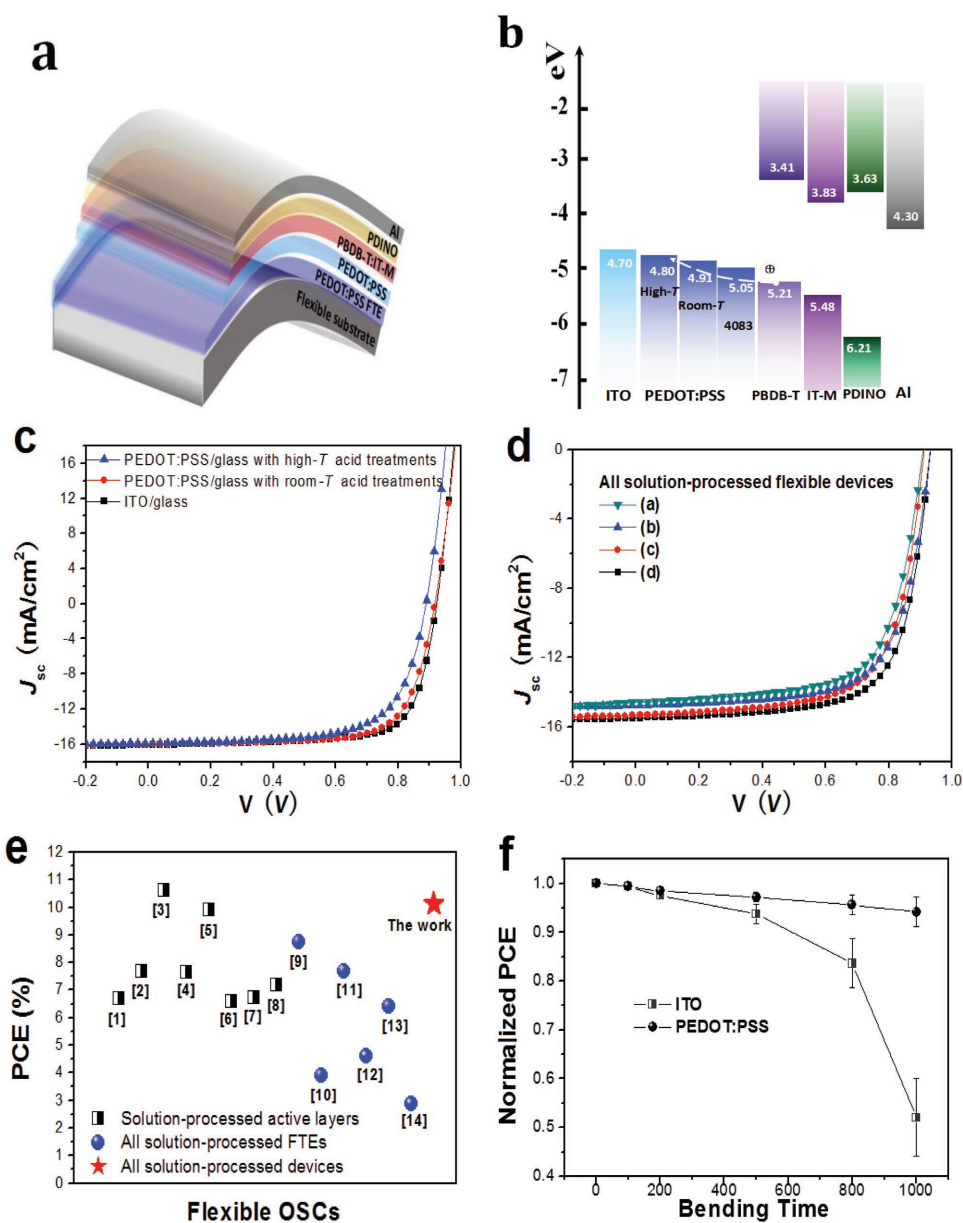


Figure 4. a) Schematic architecture of all-solution-processed flexible OSCs. b) Energy levels of the layers of flexible devices, ITO, and PEDOT:PSS films with CH_4SO_3 treatments at $\approx 140^\circ\text{C}$. c) J - V characteristics of rigid devices with the PEDOT:PSS FTEs and control devices fabricated on ITO/glass substrates. d) J - V characteristics of all-solution-processed flexible devices. e) Plotted values of PCEs of flexible OSCs reported recently. f) Decays of normalized PCEs of flexible devices in a continuous bending test: (a) flexible devices with PEDOT:PSS (≈ 80 nm)/PET and (b) reference devices with (≈ 180 nm) ITO/PET.

with CH_4SO_3 treatments at high- T ($\approx 140^\circ\text{C}$). In the study, rigid devices with PEDOT:PSS (≈ 80 nm)/glass and control devices with ITO (≈ 110 nm)/glass were fabricated first. Current-density-voltage (J - V) characteristics of the rigid devices are shown in Figure 4c under the illumination of AM 1.5G, 100 mW cm^{-2} . The rigid devices with PEDOT:PSS yielded a high PCE up to 10.60%, which is comparable to 11.01% of the control devices with ITO/glass substrates. In addition, the rigid devices with PEDOT:PSS have performed a high FF of 71.61% and J_{SC} of 16.01 mA cm^{-2} , indicating a high charge-carrier transport efficiency in the ITO-free devices. All

the photovoltaic parameters of both the devices are listed in Table 1.

Based on the above results, all-solution-processed flexible OSC devices were fabricated on the PEDOT:PSS/PET substrates. Here, one-layer (≈ 40 nm) and double-layer FTE (≈ 80 nm) were prepared for device optimization. J - V characteristics of the flexible solar cells are shown in Figure 4d. Table 1 summarizes all the photovoltaic performances of the flexible devices. It illustrates that the double-layer FTE is much superior to the one-layer FTE in device efficiency, partially contributed by the relatively low R_{sq} ($\approx 40\ \Omega\ \text{sq}^{-1}$) of the thicker FTE. Moreover,

Table 1. Photovoltaic performances of rigid devices and flexible devices based on PEDOT:PSS films and ITO, respectively.

Device	V_{OC} [V]	J_{SC} [mA cm ⁻²]	FF [%]	PCE (ave.) [%]	R_{sq} [Ω cm ²]
ITO(110 nm)/glass	0.930	16.08	76.61	11.01 (10.85)	1.5
PEDOT:PSS/glass (room-T)	0.925	16.01	71.61	10.60 (10.46)	2.3
PEDOT:PSS/glass (high-T)	0.890	15.90	67.98	9.58 (9.34)	1.8
PEDOT:PSS/PET ^{a)}	0.910	14.58	67.60	8.97 (8.83)	4.8
PEDOT:PSS/PET ^{b)}	0.930	14.75	68.71	9.42 (9.28)	3.5
PEDOT:PSS/PET ^{c)}	0.910	15.33	68.24	9.52 (9.43)	2.9
PEDOT:PSS/PET ^{d)}	0.930	15.49	70.27	10.12 (10.03)	2.9
ITO(180 nm)/PET	0.905	13.56	64.62	7.93 (7.80)	2.2

^{a)}One-layer FTE/one-layer buffer layer; ^{b)}One-layer FTE/double-layer buffer layer; ^{c)}Double-layer FTE/one-layer buffer layer; ^{d)}Double-layer FTE/double-layer buffer layer. Over ten devices were reproduced to confirm the average PCE.

the deposition of double-layer buffer layers is also critical to the flexible devices because of the achievement of better contacts at the interfaces of FTE/buffer layer and buffer layer/PBDB-T:IT-M. Figure S3 of the Supporting Information shows the wettability characteristics of PEDOT:PSS (4083) and PBDB-T:IT-M droplets. Clearly, the droplets of PEDOT:PSS (4083) showed a poor wettability with large contact angle (θ) of $\approx 44.2^\circ$ on FTE surfaces (see Figure S3a, Supporting Information), which was caused by the removal of hydrophilic PSS chains from PEDOT:PSS matrix in acid processing. The poor interface contacts lead to a low-quality coating of the buffer layers that perhaps cannot cover fully on the underlying PEDOT:PSS FTE. To solve the issue, a PEDOT:PSS (4083) buffer layer was spin-coated again on PEDOT:PSS (4083)/PEDOT:PSS FTE/PET. Obviously, a smaller θ ($\approx 32.5^\circ$) was obtained (see Figure S3b, Supporting Information), demonstrating a large improvement in wettability between the buffer layer and the FTE. Benefited to the coating of double-layer PEDOT:PSS (4083), the contact characteristic of active layers/buffer layers is remarkably improved. The contact angle of PBDB-T:IT-M is remarkably decreased from $\approx 14.0^\circ$ (Figure S3c of the Supporting Information) to $\approx 10.2^\circ$ (Figure S3d, Supporting Information). Therefore, all-solution-processed flexible devices would yield an optimal efficiency via the coatings of the double-layer FTE and the double-layer buffer layer. The flexible devices yielded the best PCE of 10.12% with V_{OC} of 0.93 V, J_{SC} of 15.49 mA cm⁻², and FF of 70.27% under illumination of AM 1.5G, 100 mW cm⁻², which is the highest value for metal-oxide-free flexible OSCs reported so far (see Figure 4e and Table S2, Supporting Information). It is believed that the all-solution-processing is important and desirable for the printing and roll-to-roll manufacturing toward cost-efficient flexible productions.

Here, the FTE and buffer layer coatings have an effect on the hole transportation and collection in devices. Therefore, the hole mobility (μ_h) of four-kinds of hole-only devices is calculated by the space charge limited current (SCLC) model using Theott–Gurney square law:^[42]

$$J_{SCLC} = \frac{9}{8} \epsilon_0 \epsilon_r \mu \frac{V^2}{L^3} \quad (1)$$

where ϵ_r is the dielectric constant of active layer materials, ϵ_0 is the permittivity of free space, L is the distance between the cathode and the anode, which is equivalent to the film thickness, and V is the applied voltage. Figure S4 of the Supporting Information presents the $V-V_{bi}$ dependence of the $J_D^{0.5}$ of the hole-only devices, where V_{bi} is the built-in voltage and J_D is the dark current density. It is calculated that the average value of μ_h is 1.05×10^{-4} , 1.33×10^{-4} , 1.73×10^{-4} , and 2.38×10^{-4} cm² V⁻¹ s⁻¹ for devices (a)–(d). The results demonstrate that the coatings of double-layer FTE and double-layer PEDOT:PSS (4083) contribute to the highest hole mobility, facilitating charge-carrier transport and collection, thus improving the efficiency of the flexible OSCs.

Moreover, on the basis of the flexible PEDOT:PSS/PET substrates, flexible solar cells are capable of affording repeated bending deformation in harsh conditions. Figure S5a of the Supporting Information shows the photography of the flexible OSC devices. To test the bending flexibility of the devices without encapsulation, a bending test in the N₂-filled glove-box was conducted. The devices were bent on cylinders at a bending radius of 5.6 mm, as shown in Figure S5b of the Supporting Information. Our results demonstrate that no obvious decrease in PCE of the flexible solar cells is observed after 200 cycles of bending tests; and the devices with PEDOT:PSS retained $\approx 94\%$ of the original value of PCE in the continuous bending test at 1000 cycles, demonstrating an excellent flexibility of the flexible devices thanks to the all-solution-processing with the nondestructive room-T gentle acid technology.

For reference, a traditional OSC device was fabricated on a commercial ITO (≈ 180 nm)-coated PET substrate. Unfortunately, the reference solar cells exhibited a low initial PCE of 7.93% with V_{OC} of 0.905 V, J_{SC} of 13.56 mA cm⁻², and FF of 64.62%, as shown in Figure S6 of the Supporting Information, which was mainly caused by the low-quality sputtering of ITO/PET that yielded a relatively low optical transparency ($\approx 81\%$ at $\lambda = 550$ nm) and electrical conductivity (≈ 2770 S cm⁻¹) measured in the work. Beside the low initial PCE of ITO-based devices, the devices showed a sharp drop in PCE in the bending test at r of 5.6 mm and just maintained $\approx 52\%$ of the initial PCE due to the intrinsic fragility of the sputtered ITO films. In addition, the flexible devices based on PEDOT:PSS without encapsulation exhibited a comparable stability with the flexible devices based on ITO, as seen in Figure S7 of the Supporting Information. Our results demonstrate that the high-performance PEDOT:PSS/PET substrates are superior to the commercial ITO/PET productions for fabricating more efficient and flexible OSC devices.

In summary, all-solution-processed flexible OSCs are fabricated on the room-T CH₄SO₃ treated PEDOT:PSS/PET substrates. Via the room-T gentle acid treatments, it endowed the PEDOT:PSS films with high optical and electrical characteristics ($T \geq 90\%$ at a broad wavelength of 450–900 nm and $\sigma = 2860$ S cm⁻¹) and smooth surfaces (RMS: 2.14 nm),

which are attributed to the removal of insulating PSS from PEDOT:PSS matrix and a better phase separation. Moreover, the mild recipe avoids destroying the plastic substrates thanks to the weak destructive characteristic of the gentle acids at room-T. For flexible device optimization, double-layer PEDOT:PSS FTE and double-layer PEDOT:PSS (4083) are critical to the flexible devices because of the achievement of good interface wettability ($\theta = 10.2^\circ$), enhanced hole mobility ($2.38 \times 10^{-4} \text{ cm}^2 \text{ V}^{-1} \text{ s}^{-1}$) as well as high R_{sq} ($\approx 40 \Omega \text{ sq}^{-1}$). Furthermore, the work function (-4.91 eV) of the PEDOT:PSS FTE matched well with the PEDOT:PSS buffer layer (-5.05 eV), benefiting to hole transportation and collection by anodes and enlarging the V_{OC} of solar cells. Therefore, the all-solution-processed flexible OSC yields the highest PCE of 10.12% with V_{OC} of 0.93 V, J_{SC} of 15.49 mA cm^{-2} , and FF of 70.27%, and maintains an excellent bending flexibility for 1000 cycles. The all-solution-processing of the components (i.e., FTEs, anode and cathode buffer layers, and active layers) is suitable for the printing, blading, and roll-to-roll manufacturing, which is promising for the penetration of cost-efficient flexible OSC productions into the markets.

Experimental Section

Materials: PBDB-T and IT-M were purchased from Solarmer Materials Inc, Beijing. Two types of PEDOT:PSS aqueous solutions (i.e., Clevious PH1000 and Clevious P VP 4083) were purchased from Heraeus, Germany.

Preparation of PEDOT:PSS FTEs: PET and glass substrates with a size of $1.5 \times 1.5 \text{ cm}^2$ were cleaned by an ultrasonic treatment in detergent, deionized (DI) water, acetone, and isopropyl alcohol (IPA), and the glass substrates were treated in a UV-ozone chamber for 10 min. A PEDOT:PSS aqueous solution (Clevious PH1000, Heraeus, Germany) doped with 0.5 vol% Zonyl FS300 was filtered using $0.45 \mu\text{m}$ syringe filter followed by spin-coating it on the underlying substrates at 2500 rpm to form pristine PEDOT:PSS films. Next, the pristine films were placed on a hot plate and were dried at 80°C for 10 min. Then, the gentle acid treatment of CH_3SO_3 was carried out at room-T for 10 min by dipping 99 wt% CH_3SO_3 droplets on PEDOT:PSS surfaces. After the gentle acid treatment, the films were washed fully by DI water and IPA three times followed by a thermal annealing at 80°C for 10 min for the obtainment of the PEDOT:PSS FTE ($\approx 40 \text{ nm}$). To prepare a double-layer PEDOT:PSS film, the PEDOT:PSS aqueous solution blended with Zonyl FS300 was spin-coated on the PEDOT:PSS/PET plastic substrates again and was conducted by the room-T gentle acid treatment mentioned above.

OSC Fabrication: OSC devices based on PEDOT:PSS electrodes and ITO films were fabricated, respectively. Prior to the deposition of a PEDOT:PSS buffer layer (Clevious P VP 4083, Heraeus, Germany), the ITO electrodes were treated by UV-plasma for 10 min to enhance surface wettability. A PEDOT:PSS (Clevious P VP 4083) solution was spin-coated at 3000 rpm on PEDOT:PSS FTEs or ITO films, and then were dried at 80°C for 10 min to form an anode buffer layer. Then, the solution of PBDB-T:IT-M (1:1 w/w, 10 mg mL^{-1} for PBDB-T) in chlorobenzene with 0.5 vol% of 1,8-diiodooctane additives was spin-coated on the surfaces of buffer layers at 1800 rpm for 60 s, followed by a thermal annealing at 100°C for 10 min in a nitrogen filled glove box. The thickness of the PBDB-T:IT-M active layers is $\approx 100 \text{ nm}$. Subsequently, PDINO in methanol solutions (1.5 mg mL^{-1}) were spin-coated on the active layers at 2000 rpm as a cathode buffer layer (thickness: 10 nm). Finally, the negative electrodes of Al (thickness: 100 nm) were thermally evaporated onto the active layer under a shadow mask at a base pressure of about 10^{-4} Pa . The shadow mask supplies eight square holes with a precise area of $2.0 \text{ mm} \times 2.0 \text{ mm}$, ensuring the area of each Al square cathode to be 4.0 mm^2 . For J - V measurements, two metal probes were contacted

well with the Al cathodes and the PEDOT:PSS electrodes or ITO, respectively.

Characterizations: Film thickness was measured by a surface profiler (Talysurf Series II). Electrical contacts were made by Ag paste and indium materials on the four corners of each PEDOT:PSS film. Film conductivity was measured by the van der Pauw four-point probe technique with a Keithley 2400 sourcemeter. Transmission spectra were taken on a Hitachi U-3010 UV-vis spectrophotometer. Film morphology was investigated by transmission electron microscopy (TECNAI G20, FEI). Compositions and chemical states of films were examined by XPS (XSAM800). Optical images were obtained using optical microscope (Nikon, Japan). Using a Keithley 2440 source-measure unit integrated with AM 1.5G solar simulator (Newport-Oriel Sol3A 450 W), J - V characteristics of the solar cells were carried out in N_2 -filled glove boxes. The light intensity was calibrated with a standard silicon detector. To evaluate the flexibility of the flexible devices, the devices were placed on cylinder surfaces with a radius of 5.6 mm and underwent a repeatable bending for a following measurement of device efficiency characteristics.

Supporting Information

Supporting Information is available from the Wiley Online Library or from the author.

Acknowledgements

This work was financially supported by the National Key R&D Program of China (2017YFE0106000 and 2016YFB0401000), the National Natural Science Foundation of China (51773212, 21574144, and 21674123), Zhejiang Provincial Natural Science Foundation of China (LR16B040002), Ningbo Municipal Science and Technology Innovative Research Team (2015B11002 and 2016B10005), CAS Interdisciplinary Innovation Team, CAS Key Project of Frontier Science Research (QYZDB-SSW-SYS030), and CAS Key Project of International Cooperation (174433KYSB20160065).

Conflict of Interest

The authors declare no conflict of interest.

Keywords

all-solution-processing, flexible organic solar cells, ITO-free, low-temperature

Received: January 3, 2018
Revised: February 28, 2018
Published online: May 16, 2018

- [1] M. Kaltenbrunner, G. Adam, E. D. Głowacki, M. Drack, R. Schwödöauer, L. Leonat, D. H. Apaydin, H. Groiss, M. C. Scharber, M. S. White, N. S. Sariciftci, S. Bauer, *Nat. Mater.* **2015**, *14*, 1032.
- [2] Y. Liu, J. Zhao, Z. Li, C. Mu, W. Ma, H. Hu, K. Jiang, H. Lin, H. Ade, H. Yan, *Nat. Commun.* **2014**, *5*, 5293.
- [3] Z. He, B. Xiao, F. Liu, H. Wu, Y. Yang, S. Xiao, C. Wang, T. P. Russell, Y. Cao, *Nat. Photonics* **2015**, *9*, 174.
- [4] Y. B. Cheng, A. Pascoe, F. Huang, Y. Peng, *Nature* **2016**, *539*, 488.

- [5] M. Kaltenbrunner, M. S. White, E. D. Glowacki, T. Sekitani, T. Someya, N. S. Sariciftci, S. Bauer, *Nat. Commun.* **2012**, *3*, 770.
- [6] Z. Liu, J. Li, F. Yan, *Adv. Mater.* **2013**, *25*, 4296.
- [7] Z. Liu, J. Li, Z. H. Sun, G. Tai, S. P. Lau, F. Yan, *ACS Nano* **2012**, *6*, 810.
- [8] X. Gu, Y. Zhou, K. Gu, T. Kurosawa, Y. Guo, Y. Li, H. Lin, B. C. Schroeder, H. Yan, F. Molina-Lopez, C. J. Tassone, C. Wang, S. C. B. Mannsfeld, H. Yan, D. Zhao, M. F. Toney, Z. Bao, *Adv. Energy Mater.* **2017**, *7*, 1602742.
- [9] H. Kang, G. Kim, J. Kim, S. Kwon, H. Kim, K. Lee, *Adv. Mater.* **2016**, *28*, 7821.
- [10] D. R. Cairns, R. P. Wittell, D. K. Sparacin, S. M. Sachsman, D. C. Paine, G. P. Crawford, *Appl. Phys. Lett.* **2000**, *76*, 1425.
- [11] S. Ye, A. R. Rathmell, Z. Chen, I. E. Stewart, B. J. Wiley, *Adv. Mater.* **2014**, *26*, 6670.
- [12] N. Espinosa, R. Garcia-Valverde, A. Urbina, F. C. Krebs, *Energy Environ. Sci.* **2011**, *4*, 1547.
- [13] J. Liu, D. B. Buchholz, R. P. H. Chang, A. Facchetti, T. J. Marks, *Adv. Mater.* **2010**, *22*, 2333.
- [14] J. Huang, C. Z. Li, C. C. Chueh, S. Q. Liu, J. S. Yu, A. K. Y. Jen, *Adv. Energy Mater.* **2015**, *5*, 1500406.
- [15] Q. Liu, J. Toudert, L. Ciannaruchi, G. Martinez-Denegri, J. Martorell, *J. Mater. Chem. A* **2017**, *5*, 25476.
- [16] C. Yeon, S. J. Yun, J. Kim, J. W. Lim, *Adv. Electron. Mater.* **2015**, *1*, 1500121.
- [17] X. Zhang, J. Wu, J. Wang, J. Zhang, Q. Yang, Y. Fu, Z. Xie, *Sol. Energy Mater. Sol. Cells* **2016**, *144*, 143.
- [18] S. I. Na, S. S. Kim, J. Jo, D. Y. Kim, *Adv. Mater.* **2008**, *20*, 4061.
- [19] J. Ouyang, *ACS Appl. Mater. Interfaces* **2013**, *5*, 13082.
- [20] Y. Xia, K. Sun, J. Ouyang, *Adv. Mater.* **2012**, *24*, 2436.
- [21] W. Meng, R. Ge, Z. F. Li, J. H. Tong, T. F. Liu, Q. Zhao, S. X. Xiong, F. Y. Jiang, L. Mao, Y. H. Zhou, *ACS Appl. Mater. Interfaces* **2015**, *7*, 14089.
- [22] N. Kim, S. Kee, S. H. Lee, B. H. Lee, Y. H. Kahng, Y.-R. Jo, B.-J. Kim, K. Lee, *Adv. Mater.* **2014**, *26*, 2268.
- [23] Z. Wu, Z. H. Chen, X. Du, J. M. Logan, J. Sippel, M. Nikolou, K. Kamaras, J. R. Reynolds, D. B. Tanner, A. F. Hebard, A. G. Rinzler, *Science* **2004**, *305*, 1273.
- [24] K.-Y. Chun, Y. Oh, J. Rho, J.-H. Ahn, Y.-J. Kim, H. R. Choi, S. Baik, *Nat. Nanotechnol.* **2010**, *5*, 853.
- [25] H. A. Becerril, J. Mao, Z. Liu, R. M. Stoltenberg, Z. Bao, Y. Chen, *ACS Nano* **2008**, *2*, 463.
- [26] X. Wang, L. J. Zhi, K. Mullen, *Nano Lett.* **2008**, *8*, 323.
- [27] D. S. Hecht, L. Hu, G. Irvin, *Adv. Mater.* **2011**, *23*, 1482.
- [28] G. Gruner, *J. Mater. Chem.* **2006**, *16*, 3533.
- [29] S. Lee, S. Shin, S. Lee, J. Seo, J. Lee, S. Son, H. J. Cho, H. Algadi, S. Al-Sayari, D. E. Kim, T. Lee, *Adv. Funct. Mater.* **2015**, *25*, 3114.
- [30] W. Zhang, Z. X. Yin, A. Chun, J. Yoo, Y. S. Kim, Y. Z. Piao, *ACS Appl. Mater. Interfaces* **2016**, *8*, 1733.
- [31] J. H. Seo, I. Hwang, H. -D. Um, S. Lee, K. Lee, J. Park, H. Shin, T.-H. Kwon, S. J. Kang, K. Seo, *Adv. Mater.* **2017**, *29*, 1701479.
- [32] J. H. Park, D. Y. Lee, Y.-H. Kim, J. K. Kim, J. H. Lee, J. H. Park, T.-W. Lee, J. H. Cho, *ACS Appl. Mater. Interfaces* **2014**, *6*, 12380.
- [33] R. Gupta, S. Walia, M. Hösel, J. Jensen, D. Angmo, F. C. Krebs, G. U. Kulkarni, *J. Mater. Chem. A* **2014**, *2*, 10930.
- [34] W. Kim, S. Kim, I. Kang, M. S. Jung, S. J. Kim, J. K. Kim, S. M. Cho, J.-H. Kim, J. H. Park, *ChemSusChem* **2016**, *9*, 1042.
- [35] J. Wang, F. Fei, Q. Luo, S. Nie, N. Wu, X. Chen, W. Su, Y. Li, C. Ma, *ACS Appl. Mater. Interfaces* **2017**, *9*, 7834.
- [36] J. Y. Oh, M. Shin, J. B. Lee, J.-H. Ahn, H. K. Baik, U. Jeong, *ACS Appl. Mater. Interfaces* **2014**, *6*, 6954.
- [37] X. Fan, J. Z. Wang, H. B. Wang, X. Liu, H. Wang, *ACS Appl. Mater. Interfaces* **2015**, *7*, 16287.
- [38] N. Kim, H. Kang, J.-H. Lee, S. Kee, S. H. Lee, K. Lee, *Adv. Mater.* **2015**, *27*, 2317.
- [39] H. Kang, S. Jung, S. Jeong, G. Kim, K. Lee, *Nat. Commun.* **2015**, *6*, 6503.
- [40] X. Fan, B. G. Xu, S. H. Liu, C. H. Cui, J. Z. Wang, F. Yan, *ACS Appl. Mater. Interfaces* **2016**, *8*, 14029.
- [41] K. Sun, P. C. Li, Y. J. Xia, J. J. Chang, J. Y. Ouyang, *ACS Appl. Mater. Interfaces* **2015**, *7*, 15314.
- [42] J. W. Jung, W. H. Jo, *Adv. Funct. Mater.* **2010**, *20*, 2355.